Open Journal of Clinical & Medical Images

www.jclinmedimages.org

ISSN: 2833-2725

Short Commentary

Open Access, Volume 4

Spatial distribution of calcium chemical bonds in the intact area of femur under osteoarthritic conditions

AA Pavlychev[1]*; XO Brykalova[1]; AA Cherny[2]; AV Korneev[1]; NN Kornilov[2]

[1]St. Petersburg State University, Saint Petersburg, 198504, Russia.

[2]National Medical Research Center for Traumatology and Orthopedic, Saint Petersburg, 195427, Russia.

***Corresponding Author: AA Pavlychev**

St. Petersburg State University, Saint Petersburg, 198504, Russia.

Email: a.pavlychev@spbu.ru

Received: Sep 10, 2024

Accepted: Oct 04, 2024

Published: Oct 11, 2024

Archived: www.jclinmedimages.org

Keywords: Biotechnology; 3D imaging; Osteoarthritis; XPS; Native Bone; Bone Nanostructure; Calcium hydroxy-apatite.

Abstract

Applying X-ray photoelectron spectroscopy to human femur, we see a distinct spatial inhomogeneity in the distribution of Ca^{2+} bonds not only on the surface of osteoarthritis damaged knee department, but also in the depth of subchondral bone. The spectroscopic data analysis has demonstrated strong site dependent distortions of calcium chemical states compared to those in calcium hydroxyapatite crystal. These distortions are essential even in the intact area and reach a maximum at depth of 50-200 μm below the surface monolayer. This inhomogeneity cannot be directly assigned with the chemical reactions on the interphase of damaged cartilage with mineralized bone. We assume that it is originated by fatigue strains in the mineral phase. Thus, the site dependent peculiarities of chemical bonding in femur are a product of two counter processes directed from both the cartilage mineral boundary inward and the bulk of subchondral bone towards its proximal surface. Further experimental studies of native bone together with 3D modeling of its atomic molecular architecture are discussed.

Introduction

The optimization of locomotor processes performed against the gravity forces is achieved by a hierarchical organization of the vertebrate skeleton. The organization provides a biologically appropriate level of resistance of bone structures to mechanical loads during movement [1-5]. This concept is confirmed not only by the very fact of the existence of vertebrates in nature, but also by the preservation of the main morphological features of the skeleton from the nano to the macroscopic scale for more than 80 million years [6]. According to J. Wolff [7], it is mechanical loads that arise during the execution of locomotors functions that control the orientation of bone structures.

The easily tunable properties of hexagonal calcium hydroxyapatite (CaOH-Ap) $Ca_{10}(PO_4)_6(OH)_2$ under the influence of chemical substitutions, vacancies and water molecules make it unrivaled in comparison with other minerals. Changes in the stoichiometry of $Ca_{10}(PO_4)_6(OH)_2$ determine biologically significant characteristics such as solubility, hardness, brittleness, deformability, thermal stability and crystallite size [8-11]. In particular, the replacement of phosphate ions with carbonate ions leads to deformations of the crystal lattice, which, increasing the solubility of CaOH-Ap, limit the size of its particles [9,10]. Thus, biochemical reactions interact with skeletal biomechanics and results in the site-dependent transformation of the atom-molecular architecture of bone under physiological and pathogenic conditions.

To what extent does the Wolf's paradigm control the bone architecture at the nano level? The X-ray linear dichroism observed near the Ca^{2+} $2p_{3/2,1/2}$ ionization thresholds in the cortex of femur [12], highlights a correspondence between the directions of bone long axes and the gravity force lines with the orientation of calcium bonds.

X-ray Photoelectron Spectroscopy (XPS) and X-Ray Diffraction (XRD) point at a more complicated situation in Osteoarthritis (OA) damaged areas [13,14] due to the interplay of biochemical and biomechanical processes on the cartilage – mineral inter-

phase. The most significant deviations of calcium bonds compared to CaOH-Ap are detected [13,14] not inside the sclerosis bone areas, inside which mechanical loads are maximum, but near them where the mineral phase contacts with broken-cartilage. The situation was respectively associated with catalytic reactions as their ratio increases in the vicinities. The concentration of Ca^{2+} ions in chemical states not resident in CaOH-Ap is found (i) insignificant in the intact area, (ii) dominating in the contact of mineral with broken-cartilage and (iii) reduced inside the area of sclerotic bone with the complete loss of the cartilage. Pay attention that the probing depth of Ca^{2+} states by XPS is ≈10 nm. Hence, the site-dependence of Ca^{2+} in homogeneity refers to the surface monolayer of CaOH-Ap crystallites, the mean size of which is about 10 nm [15].

How deep does the identified site dependence persist? To answer the question our focus is on changes in chemical bonds of Ca^{2+} located deeper inside the subchondral bone. For this purpose, the depth-dependence of Ca^{2+} was probed using XPS. We have expected to observe a monotonous transformation of calcium bonds in the intact area, since apatite-like Ca^{2+} states play a dominant role in the surface layers on both the proximal and distal sides of the saw-cuts [13,14]. But unexpectedly, the measurements have demonstrated a significantly non-monotonic variations of calcium bonding, namely, a hidden interlayer with well pronounced non-apatite calcium states is detected.

Samples and methods

Samples preparation

The medial and lateral condyles of the femur resected during total knee arthroplasty in patients with medial compartmental knee OA were used here as samples to study changes in the local electronic and atomic structure of the subchondral bone. (Figure 1) displays a radiograph of the OA-damaged knee joint. The sample of healthy bone is a saw-cut of the condyle of femoral bone, not subjected to excessive loads, with intact cartilage (area 1 in Figure 1). The bone sample of damaged area is a saw cut of the same femoral bone, subjected to excessive mechanical stress due to the development of OA and deformity in the joint, with full-layer loss of cartilage. The area referring to the sclerotic bone is labeled as 2 in (Figure 1), left panel. Just outside 2 there is a contact region with erased cartilage marked as 3. Such a choice of the objects makes it possible to analyze the subsequence of spatial changes in the bone under the action of mechanical loads.

The bone samples were prepared at the R.R. Vreden National Medical Research Center of Traumatology and Orthopedics of the Ministry of Health and Social Development of the Russian Federation. The study was also approved by the Local Ethical Committee of the Center. All patients have signed informed a consent form.

To prepare the bone samples for the XPS measurements, in the beginning, the bone saw-cuts were cleaned of cartilage tissue using a gentle mechanical treatment with a scalpel, to subchondral bone plate. Then, to degrease the cuts and remote the myeloid contents from the trabeculae of the spongy layer, the samples were kept for 4 days in a bath with an aqueous 33% hydrogen peroxide solution (H_2O_2) mixed in a 1:1 ratio with hot water (60°C) and with the addition of 5 ml of 10% aqueous ammonium hydroxide solution (NH_4OH). This mixture was replaced daily. To complete the cleaning process the samples were placed for one day in distilled water, changing it every 6 hours. For the XPS measurements the samples were additionally subjected to heating at 180°C for 2 days in thermostat to depress the water evaporation. Just before the XPS measurements their argon-ions-cleaning was used.

To investigate the variations of calcium chemical states depending on the depth, additional sections of the saw-cuts were made in the direction from their proximal to the distal side. These sections are shown with red lines in (Figure 1) (right panel). To define them in more detail, we introduce a coordinate system X, Y, Z in which the X and Y axes are located on the proximal side and oriented as it is shown in the (Figure 1), and the Z axis is directed deep into the saw-cuts.

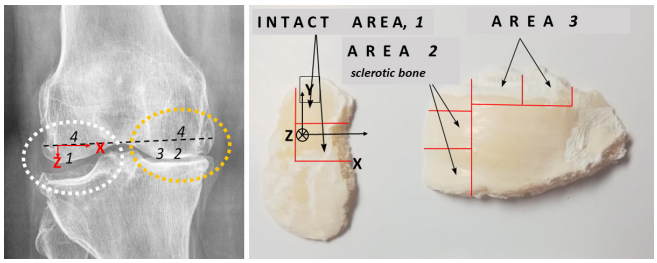

Figure 1: Left panel: OA-damaged knee joint: different areas on proximal side of the femur: intact 1, sclerotic bone 2, and its vicinities 3. Dots show the position of the distal side (area 4) of saw-cuts under study. Right panel: photos of the bone samples, the dispositions of additional sections normal to the proximal to the distal side are marked with red lines. The X, Y, Z coordinates are shown. Z axis is directed down.

Experimental methods

The XPS measurements were performed for the bone samples in the intact area by using the photoelectron spectrometer Thermo Fisher Scientific Escalab 250Xi. No sample charging or decomposition effects were detected during the studies. The measurements were recorded several times and have demonstrated a good reproducibility.

XPS is a well-known method providing sensitive probing of chemical bonds in surface layers [16,17]. In our case, the probing thickness is estimated at ≈10 nm. This value is determined by the peculiarities of PE waves propagation in bone tissue. To examine the chemical bonding below the upper monolayer, the Ca^{2+} $2p^{-1}_{3/2,1/2}$ photoemission from the surface of the additional YZ (and XZ) sections are carried out. Within this experimental geometry, the depth measurement step along the Z axis is determined not by the PE waves propagation in bone tissue, but by the size of the spectrometer focal spot, the radius of which is about 200 micrometers.

The measured Ca^{2+} $2p^{-1}_{3/2,1/2}$-PE lines referring to the YZ section (Figure 1) as functions of the depth *z* are exhibited in (Figure 2). These spectra specify the photoelectron emission from Ca^{2+} ions located on different spots on the section normal to the proximal side. The Ca^{2+} $2p^{-1}_{3/2,1/2}$ spectra in (Figure 2) are normalized to the total array of the Ca $2p_{3/2,1/2}$ and Ca $2p_{1/2}$ spin-orbit split PE signals. Apart of their similarity, we also see the different energy positions and shapes of the signals. To document the deviations of the spectroscopic parameters as a function of

z, the Voigt-functions-fit analysis of the experimental data was performed.

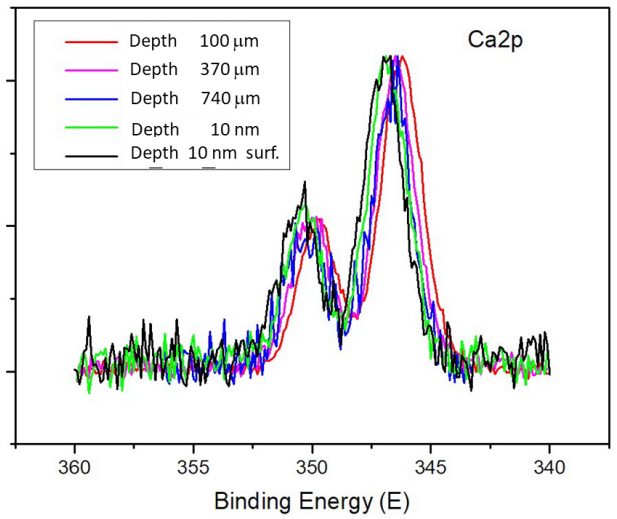

Figure 2: A depth dependence of the experimental Ca^{2+} $2p^{-1}_{3/2,1/2}$ PE lines in intact area. Green and black curves demonstrate the surface spectra (XY plane), black line the data from reference [13].

Experimental data analysis

Earlier the Voigt-functions-fit analysis was successfully used to specify changes in the atom-molecular architecture of bone under physiological and pathogenic conditions (see, e.g. [13,18,19]). It makes it possible to extract the Ca $2p_{3/2,1/2}$ electron BEs, the Lorentzian and Gaussian Full-Width-At-The-Half-Maximum (FWHM) and to examine the composition of the PE bands. The Lorentzian width is determined mainly by the Ca^{2+} 2p-hole life time, whereas the Gaussian width depends on the bandwidth of photon source and on the inhomogeneous imperfectness of CaOH-Ap nanocrystals.

The single-Voigt-function-fit approximation reproduces precisely the spin-doublet shape of the Ca $2p^{-1}_{3/2,1/2}$ PE lines in CaOH-Ap, carbonate calcium hydroxyapatite and in areas 1 and 4, but not in areas 2 and 3 [13,14], for which the number of Voigt functions increased, so that one of them coincided with the function that reproduces the signal from the intact area.

The analysis of the Ca^{2+} $2p^{-1}_{3/2,1/2}$ PE line shape distortions and energy shifts allows us to quantify the site-dependence of CaOH-Ap-to-bone deviations in the electronic and atomic structure and calcium bonding. The analysis has shown that in OA-damaged areas 2 and 3 the PE bands are basically composed from two main components denoted as Ca^{2+}(A) and Ca^{2+}(X). The Ca^{2+}(A) component refers to apatite-like calcium states. It dominates in CaOH-Ap and healthy bone but its role drops in OA-damaged areas.

The weakly bound non-apatite Ca^{2+}(X) becomes essential in X-ray photoemission from the proximal side in OA-damaged areas and can be roughly attributed to calcite-like states [13]. Note, that in some cases, the highly bound non-apatite Ca^{2+}(Y) can be also detected. But in the present study, it does not appear. The extracted energy positions $E_{A(X)}$ of the Ca^{2+}(A) and Ca^{2+}(X) components, respectively, and their FWHM $W_{A(X)}$ as well as their relative contributions (R) to the total signal are collected in Table 1.

Table 1: The composition and the spectroscopic parameters $E_{A(X)}$ and $W_{A(X)}$ of Ca^{2+} $2p^{-1}_{3/2,1/2}$ PE lines as a function of depth.

#	Space	Components	$E_{A(X)}$ ($W_{A(X)}$) of Ca^{2+} $2p_{3/2}$ component	*R*
1	HAP	A	347,2(1,6)	100%
2	Surface, z≈10 nm (Proximal side ref. [13])	A X	347,0(1,9 Traces	>95%
3	Surface, z≈10 nm, Monolayer; sample from this work	A X	346,9(1,9) 346,2(1,9)	86% 14%
4	z≈100 μm	A X	346,9 (1,95) 346,2 (1,95)	12% 88%
5	z≈370 μm	A X	346,9(1,76) 346,2(1,76)	42% 58%
6	z≈740 μm	A X	346,9(1,8) 346,2(1,8)	60% 40%
7	z≈150 mm Distal side	A X	346,9(1,9) Traces	>95%

Analyzing the dependence of Ca^{2+} $2p^{-1}_{3/2,1/2}$PE lines on z we infer that calcium bonds undergo substantial non-monotonous changes in mineralized bone. The changes indicate a depopulation of Ca^{2+}(A) at the initial stage of immersion into the bone, and its percentage comes over a minimum at the depth z_{min} ≈ 100 μm, and, then, the percentage increases at $z>z_{min}$. This non-monotonic distribution of Ca^{2+}(A) in subchondral bone is a rather surprising observation. It is unclear how the interlayer of the non-apatite calcium states, remote from the organic-mineral interphase, is formed.

(Figure 3) shows how the percentage of the apatite-like Ca^{2+}(A) in bone varies with depth in the intact area within the YZ section. z=0 corresponds to its upper monolayer. One may see that Ca^{2+}(A) dominates both near surface z<1 μm and in the bulk with z>1 μm, however, there is an interlayer 1 μm < z < 10^3 μm with a noticeable destruction of calcium bonds. Within the interlayer at a depth of 10-150 μm, the contribution of the non-apatite Ca^{2+}(X) increases up to 88%. Pay attention to the logarithmic depth scale. So, we see 3 characteristic layers: first (I), the surface apatite-like layer, the second, (II) the intermediate layer of disturbed apatite calcium and, finally, (III) the apatite-like bulk of the subchondral bone. Such a schematic division of the bone saw-cut by depth is shown in (Figure 3).

The formation of the disordered intermediate layer cannot be directly related to the influence of catalytic reactions occurring at the cartilage-mineral interphase border, since, firstly, this interlayer is separated from the border by a superficial undamaged layer and, secondly, it is observed even in the intact area.

We suggest that the appearance of this damaged layer may be related to fatigue deformations that accumulate in the mineralized phase with age. However, this assumption requires further probing and research. Considering that (i) no other crystalline phase except CaOH-Ap is observed in bone [14] and (ii) the fraction of non-apatite calcium bonds in it is a quantitative marker of structural deformations in the crystal lattice, we conclude that it is the short-range order that is a subject to the greatest distortions, and the distortions are predominantly localized at the boundaries of CaOH-Ap nanocrystals located both on the proximal side and in the depth of the subchondral bone. The appearance of local structural defects invokes a redistribution of mechanical loads in mineralized bone and contributes to the formation of microcracks in it.

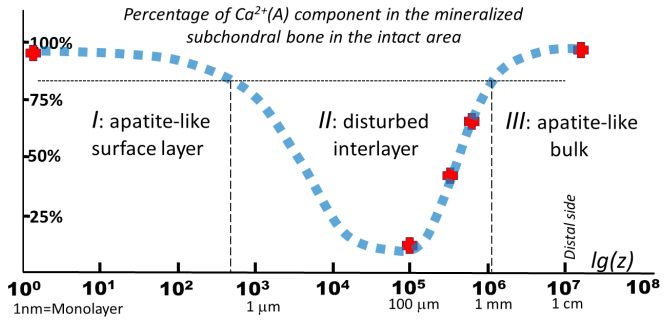

Figure 3: Variations of apatite-like Ca^{2+}(A) percentage as function of depth. Figure caption is always placed below the illus-tration. Short captions are centered, while long ones are justified. The macro button chooses the correct format automatically.

(Figure 4) illustrates the spatial inhomogeneity of calcium bonds in subchondral bone. The left and central panels display schematically the distributions of apatite-like Ca^{2+}(A) on the proximal side (XY plane) in intact and OA-damaged areas. The images present the average data obtained for 12 patients. The right panel displays a map of the Ca^{2+}(A) distribution in depth (YZ plane) in the intact area (logarithmic scale is used).

The left panel shows the almost homogeneous distribution of Ca^{2+}(A) that plays a dominating role in the intact area on the proximal side. The central panel demonstrates the strong distortions of apatite-like bonds on the proximal side inside the sclerotic bone (areas 3 and 2) and around it. Specifically, the distortions in the vicinities (area 3) are higher than inside it (area 2). The right panel exhibits the dependence of calcium chemical bonds on depth and the appearance of the hidden interlayer with their strong distortions, where Ca^{2+}(X) is a dominating unit.

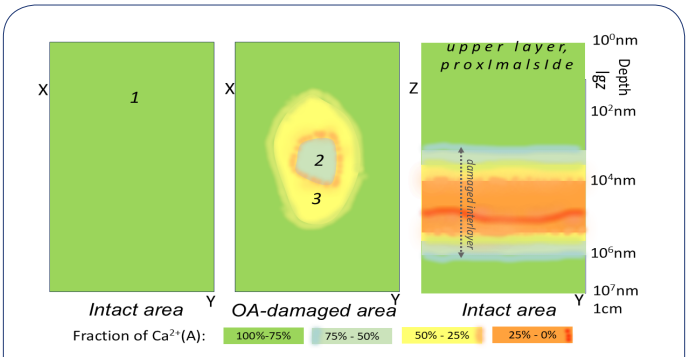

Figure 4: The schematic distribution of calcium states in the XY plane in the intact (left panel) and OA damaged (central panel) areas on the proximal side. Right panel presents the distribution in the YZ plane in the intact area. Strong depth-dependence of calcium states is clear visible.

Conclusion

The XPS probing of subchondral bone under OA conditions has demonstrated that in addition to the distortions of apatite-like calcium states in the upper monolayer on the proximal side there is another region with a dominance of disturbed non-apatite calcium bonds, which is located in the bulk. The case study has shown that this region lies at a depth of 50-200 μm below the upper monolayer and the concentration of Ca^{2+}(X) in it reaches even higher value than that on the proximal side in the OA-damaged areas. The mechanism that leads to the rupture of apatite-like calcium bonds in this region cannot be directly linked to chemical reactions occurring at the "destroyed cartilage-mineral" interphase, since it is separated from the interphase boundary by a weakly disturbed apatite layer.

We assume that the nature of these deep-seated distortions is closely related to the accumulation of fatigue deformations. The formation of the extended structural defects in bulk invokes a redistribution of mechanical loads inside the mineralized bone and gives rise to microcracks in it.

Preliminary analysis of calcium bonds in the bone depth corresponding to the areas 2 and 3 indicates a tendency for the areas with non-apatite bonds to merge at the phase boundary and in depth. Thus, it can be expected that the development of OA is accompanied by the expansion of damaged areas in the directions from the interphase boundary inward and from the bulk outward. On this background further interdisciplinary research of native bone together with 3D modeling of its atomic-molecular architecture under physiological and pathogenic conditions becomes very important. These studies allow us to test in more detail the assumption of the fusion, construct and inspect 3D maps of the local bone destruction on the nanoscale, disclose the mechanisms of spatiotemporal changes in bone under different conditions and develop new biotechnologies of bone regeneration.

Acknowledgment: This research was carried out with the support of the Centre for Physical Methods of Surface Investigation and Centre for Diagnostics of Functional Materials for Medicine, Pharmacology and Nanoelectronics at St. Petersburg State University. This work was supported by Russia Science Foundation, Grant 23-29-00172.

References

1. Frost HM. Defining osteopenias and osteoporoses: Another view (with insights from a New Paradigm). Bone. 1997; 20: 385-391.

2. Prendergast PJ. Mechanics applied to skeletal ontogeny and phylogeny. Meccanica. 2002; 37: 317-334.

3. Skerry TM. One mechanostat or many? Modifications of the site-specific response of bone to mechanical load-ing by nature and nurture. J. Musculoskelet Neuronal Interact. 2006; 6: 122-127.

4. Skerry TM. The response of bone to mechanical loading and disuse: Fundamental principles and influences on osteoblast/osteocyte homeostasis. Archives of Biochemistry and Biophysics. 2008; 473: 117-123.

5. AS Avrunin, AA Pavlychev, YI Denisov-Nikolskij, AA Doktorov, AS Vinogradov, et al. Morphological character-istics of the nanolevel mechanisms that determine stretch and physical and chemical properties of bone tissue, Morphology. 2016; 150: 77-83.

6. Casalbou S, Combes C, Eichert D, Rey C. Adaptative physicochemistry of bio-related calcium phosphates. J. Mater. Chem. 2004; 14: 2148-2153.

7. Wolff J. Das Gesetz der Transformation der Knochen; Hirschwald: Berlin. 1892.

8. Doktorov AA, Denisov-Nikolski Yu I Zhilkin BA. [Strukturnaia organizatsiia kostnogo minerala.]Byul. eksperim. Meditsiny [Bull Exp Biol Med]. 1996; 122(12): 687-691.

9. Knothe Tate ML. Multiscale computational engineering of bones: State-of-the-art insights for the future. In book: Engineering of functional skeletal tissues. 2007; 141-160.

10. Tsai TWT, Chan JCC. Recent Progress in the Solid-State NMR Studies of Biomineralization. Chapter 1. An-nual Reports on NMR Spectroscopy. 2011; 73: 1-61.

11. AS Avrunin, YI Denisov-Nikolskij, AA Doktorov, Yu A Krivosenko, DO Samoilenko, et al. The effect of water, various incorporations and substitutions on physical and chemical properties of bioapatite and mechanical proper-ties of bone tissue, Traumotology and Orthopedics. 2015; 3(77): 37-50.

12. AS Konashuk, XO Brykalova, NN Kornilov, EO Filatova, AA Pavlychev. Hierarchy-induced X-ray Linear Dichroism in Cortical Bone, Emergent Materials. 2020; 3(4): 515-520.

13. XO Brykalova, NN Kornilov, YA Rykov, AA Cherny, AA Pavlychev. Site-Dependent Peculiarities of Calcium Bonds in Bone Tissue, J. Phys. Chem. Lett. 2020; 11: 7839-7842, doi: 10.1021/acs.jpclett.0c01722

14. Andrey A Pavlychev, Xenia O Brykalova, Aleksandr A Cherny, Anatoliy V Korneev, Nikolai N Kornilov. Spa-tiotemporal Changes in Atomic and Molecular Architecture of Mineralized Bone under Pathogenic Conditions, Crystals. 2023; 13(3): 381.

15. Pavlychev AA, Avrunin AS, Vinogradov AS, Filatova EO, Doctorov AA, et al. Rostov Local electronic struc-ture and nanolevel hierarchical organization of bone tissue: theory and NEXAFS study, Nanotechnology. 2016; 27: 504002-1-8.

16. Baer DR, Artyushkova K, Richard Brundle C, Castle JE, Engelhard MH, et al. Practical guides for x-ray pho-toelectron spectroscopy: First steps in planning, conducting, and reporting XPS measurements. Journal of Vacuum Science & Technology A: Vacuum, Surfaces, and Films. 2019; 37(3): 031401.

17. Nesbitt HW, Bancroft GM, Pratt AR, Scaini MJ. Sulfur and iron surface states on fractured pyrite surfaces. American Mineralogist. 1998; 83(9-10): 1067-1076.

18. Xenia O Brykalova, Nikolai N Kornilov, Alexander A Cherny, Yuri A Rykov, Andrey A Pavlychev. Electronic and atomic structure of subchondral femoral bone in intact and osteoarthritic knee compartments // Eur. Phys. J. D. 2019; 73: 113.

19. Xenia Brykalova, Nikolai Kornilov, Andrey Pavlychev. The peculiarities of charge distribution and spatiotem-poral changes in electronic and atomic structure of bone tissue, J. Mater. Chem. A. 2022; 10: 22686-22693.